Density functional theory study of electronic structures in lithium silicates: Li_2SiO_3 and Li_4SiO_4

Tao Tang[a],[*] and De-Li Luo[a],[b],[*]

[a] *National Key Laboratory for Surface Physics and Chemistry, P. O. Box 718-35, Mianyang 621907, China*
[b] *China Academy of Engineering Physics, P. O. Box 919-71, Mianyang 621900, China*

Abstract. Lithium silicates, such as Li_2SiO_3 and Li_4SiO_4, are considered as favorable candidates for the tritium breeding materials of a nuclear fusion reactor. Their bulk electronic properties and mechanics are important for the tritium behavior and tritium breeding blanket designs. We have studied the structural and electronic properties of Li_2SiO_3 and Li_4SiO_4 bulks using density functional theory (DFT) within generalized gradient approximation (GGA). The calculated crystal parameters are well consistent with the experimental results. The electronic band energy calculations show that Li_2SiO_3 and Li_4SiO_4 are insulators with a band gap of about 5.36 and 5.53 eV, respectively. Their valence band properties are mainly determined by the oxygen $2p$ orbital electrons. The two types of oxygen atoms, nonbridging oxygen (NBO) atoms and bridging oxygen (BO) atoms, in Li_2SiO_3 reveal significantly different electron distribution of oxygen $2p$ orbital. The Si $3s$ and $3p$ hybridization is observed in Li_2SiO_3, but not in Li_4SiO_4. In both lithium silicates, the electronic density increases more steeply around Li and Si atom sites compared with that around O atoms. Additionally, the mechanical properties of both lithium silicates were calculated and discussed first time.

PACS: 61.50.Lt, 63.20.dk, 63.70.+h, 64.10.+h

Key words: electronic structure, density functional theory, lithium silicates, fusion

1 Introduction

The breeding blanket material is the key of a fusion reactor because of the production of tritium which is required by fusion reactors of the deuterium-tritium type [1–3]. This material should have a number of properties, such as (a) low electric conductivity, (b) high

mechanical resistance, (c) high thermal stability, (d) potentially high tritium generation and (e) fast tritium release [2], to be considered as a possible candidate for the tritium breeding blanket. Keeping these properties in mind, some lithium-containing ceramics, including Li_2O, $LiAlO_2$, Li_4SiO_4, Li_2SiO_3, Li_2ZrO_3, Li_2SnO_3 and more recently Li_2TiO_3, have been proposed [4–17]. Each of these materials has advantages and disadvantages that should be kept in mind towards choosing a material to use. Among these ceramics, lithium silicates, Li_4SiO_4 and Li_2SiO_3, have attractive natures for lithium density, compatibility with the structure materials, release performance of bred tritium and so forth. However, there are many characteristics still not determined, like diffusion constants of tritium in the bulk and on the surface, determination of precise parameters defining adsorption and desorption, identification of mechanism of tritium release and how the generation and tritium release is affected by the defects of the crystalline structure.

Recent advance in the computer performance and computer codes makes it possible to study the chemical nature of condensed materials, such as metal, alloy, ceramics and others, by *ab initio* calculation that is a powerful tool to know how the electrons affect the property of substance. Actually, in order to understand the natural properties of lithium-based ceramics, the tritium localization in and the interaction mechanism with the surface and defects of lithium-based ceramics, especially for Li_2O, a lot of theoretical investigations based on the quantum chemistry calculation had been performed soon after solid tritium breeding concept emerging in fusion energy development [18–27]. Among these investigations, a lot of works were carried out for the bulk ground state properties, various defects formations and migrations, and the hydrogen isotopes absorption and desorption behaviors on the surface of lithium oxide (Li_2O) [18–25].

Nevertheless, only a few theoretical studies are available regarding the ground state properties and dynamics of the tritium in ternary lithium-containing ceramics due to their structural complications. For example, Campos studied two possible substitutional sites in the positions occupied by lithium atoms [26] and two octahedral sites [27] for tritium atoms in the Li_2TiO_3 structure using a quantum chemistry approach. It was found that the tritium atoms in lithium titanate preferably occupied in octahedral sites near lithium layers and followed by substitutional sites in lithium layers and titanium layers, respectively. These studies can give clues for understanding of behavior of tritium bred in the crystals or on the surface of breeder materials.

Although some efforts [28–30] had been made to study the hydrogen isotopes or water molecular adsorption on and desorption from lithium silicates surface based on the cluster model using quantum chemistry method, few studies have been done regarding the tritium behavior or ground state properties in Li_2SiO_3 and Li_4SiO_4 bulks. Ching *et al*. [31] studied the electronic structures of Li_2SiO_3 and $Li_2Si_2O_5$ and examined their electronic density of state (DOS) by density functional calculations in a periodic system based on the experimental crystal structure. Munakata *et al*. [32], probably the first one, studied the electron state in Li_4SiO_4 crystal using *ab initio* calculation implemented in the CRYSTAL98 code, and reported the charge Mulliken population analysis and the electron density of state (DOS). However, the further investigation has not been reported as for

now.

In order to understand the tritium and helium behavior in lithium silicates, which is very important for the ITER TBM design, we will perform theoretical and experimental studies on this issue. As the first step, an *ab initio* caculation within density functional theory will applied to explore the electronic structures of the bulk Li_2SiO_3 and Li_4SiO_4. Based on these data, the energetic and mechanical properties of the lithium silicates crystal will be evaluated.

2   Calculation details

In this study we carried out first principle calculations based on density functional theory (DFT), as implemented in CASTEP code which uses a plane wave basis set for expansion of effective single particle Kohn-Sham energy [36–39]. Ultrasoft pseudopotentials were used to describe the interactions of ionic core and valence electrons. Valence states considered in this study are including Li $1s^22s^2$, Si $3s^23p^2$ and O $2s^22p^4$. The generalized gradient approximation (GGA) within Perdew and Wang (PW91) scheme [40] was employed to evaluate exchange-correlation energy. A kinetic energy cut-off 400 eV was used for plane wave expansions in reciprocal space of Li_2SiO_3 and Li_4SiO_4, respectively. Energy calculations in the first irreducible Brillouin zone were performed using a special k point sampling methods of Monkhorst-Pack scheme and set as $5\times5\times5$ and $3\times5\times5$ for Li_2SiO_3 and Li_4SiO_4, respectively. BFGS optimization method was used to find the ground state of Li_2SiO_3 and Li_4SiO_4 crystals which both atom positions and lattice parameters were optimized simultaneously [41]. Total energy changes were finally reduced less than 1×10^{-5} eV/atom, and Hellman-Feynman forces acting on atoms were converged less than 0.03 eV/Å. In order to calculate binding energy of these structures, we also carried out calculations for Li, Si and O crystal in order to get bulk binding energy values of pure elements. Total energy of isolated Li, Si and O atoms were directly achieved from CASTEP output files.

Usually, binding energy is defined as

$$E_b(Li_xSiO_y) = \frac{E_{tot}(Li_xSiO_y, \text{cell}) - xnE_{iso}(Li) - nE_{iso}(Si) - ynE_{iso}(O)}{n}, \tag{1}$$

where $E_b(Li_xSiO_y)$ is binding energy of Li_xSiO_y per formula, $E_{tot}(Li_xSiO_y, \text{cell})$ is total energy of calculated cell, $E_{iso}(X)$ represents total energy of isolated atom X, n is total number of Li_xSiO_y formula contains in crystal.

3   Results and discussion

3.1   Crystalline structures optimization

Like Na_2SiO_3, at ambient pressure and temperature, Li_2SiO_3 has an orthorhombic structure with lattice constants, as shown in Table 1, (a,b,c)=(9.396, 5.396, 4.661) (unit=Å)

Table 1: The experimental and calculated crystal structural parameters of Li_2SiO_3 and Li_4SiO_4.

Species	Space group		Expt. (Å)	Calc. (Å)	Formula unit Z
Li_2SiO_3 (orthorhombic)	$Cmc2_1$	a	9.396	9.487	4
		b	5.396	5.450	
		c	4.661	4.713	
Li_4SiO_4 (monoclinic)	$P2_1m$	a	11.546	11.725	14
		b	6.090	6.092	
		c	16.645	16.800	
		β	99.5°	98.6°	

[space group $Cmc2_1$ (No.36)] [33]. It has four molecular units (24 atoms) per cell, as shown in Fig. 1, consisting of one type of Li atoms with site of 8*b*, one type of Si atoms with site of 4*a*, and two types of O atoms with site of 8*b* and 4*a*, respectively. The experimental coordinates of Li, Si and O atoms are listed in Table 2. Like its' counterparts in sodium silicates, the lithium metasilicate has chains of SiO_4 tetrahedra with lithium atoms floating around the chains. There are two type of oxygen atoms in this structure, the non-bridging oxygen atoms (NBO) or O1 (8*b*) and bridging oxygen atoms (BO) or O2 (4*a*). The three nearest Li atoms to NBO O1 have 1.937, 1.938 and 1.955 Å while the fourth Li atom is 2.755 Å from O1. The closest distance between Li atom and a BO O2 is 2.170Å. The Si-O_1 bond length is 1.606 Å while Si-O_2 is 1.700 and 1.702 Å, alternately.

Li$_4$SiO$_4$ is one complicated ternary lithium silicate. Völlekle probably first reported the crystal structure of Li_4SiO_4. According to their report [34], the crystal structure of Li_4SiO_4 is the monoclinic with unit cell a=5.14 Å, b=6.10 Å, c=5.30 Å and β=90.5°. The structure is reported to contain six crystallographiacally different Li atoms. All the lithium sites are partially occupied with occupancy factor ranging from 1/3 to 2/3. However, this crystal structure is not suitable for *ab initio* studies of electron states in Li_4SiO_4, since the location of Li atoms in the crystal is not clear because of the partial occupancy of Li in the crystal. After the report mentioned above, Tranqui *et al*. [35] redefined the structure of Li_4SiO_4 crystal by analyzing their X-ray diffraction data. The reported structure, as shown in Table 1, is also monoclinic with space group $P2_1/m$, but the unit cell is a=11.546 Å, b=6.090 Å, c=16.645 Å, and β=99.5°. They called it "super structure", which contains 14 formula units (seven different units) and is seven times as large as the cell described by Völlenkle *et al*. [33]. Additionally, this "super structure"accurately reproduces the stoichiometry of the chemical formula of Li_4SiO_4 and is thought to be reasonable and used in the *ab initio* study of this work. Fig. 2 shows the unit cell (super structure) mode. The positional parameters of Li, Si, and O atoms are referenced to those given by Tranqui *et al* [35]. This structure has isolated SiO_4 tetrahedra and Li atoms floating around them, in which there are one type of Si atoms (7 atoms with site of 2f), two types of O atoms: 7 atoms with site of 4f and 14 atoms with site of 2e, and two types of Li atoms: 9 atoms with site of 4f and 10 atoms with site of 2e. Thus, total 126 atoms (56 Li, 14 Si and 56 O) were taken into consideration in the *ab initio* calculation. The Si-O bond length is variable

from 1.609 to 1.699 Å.
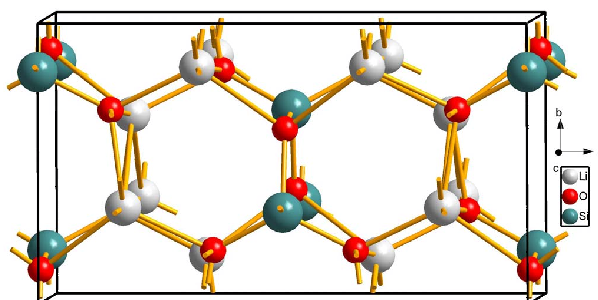
Figure 1: The unit cell of Li_2SiO_3 crystal.
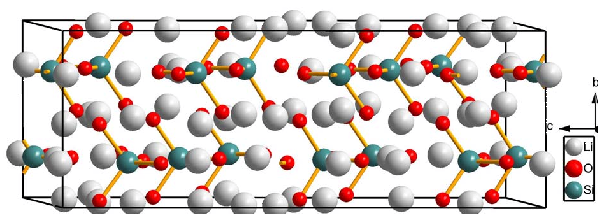
Figure 2: The crystal model (side view) of Li_4SiO_4 super structure projected along (100). The smallest, moderate and largest balls represent O, Si and Li atoms, respectively.

Since the accuracy of the first principle calculations may dependent on many parameters, such as kinetic energy cut off value for plane wave expansions, exchange-correlation energy scheme and k point grid, etc. We calculated the variations of binding energy of Li_2SiO_3 and Li_4SiO_4 as a function of energy cut off values, the LDA within LZ-CP (LDA + LZ-CP)and GGA within PBE and PW91 (GGA + PBE and GGA + PW91) schemes are used in order to assure the accuracy of our results. Although there is difference between GGA+PBE and GGA+PW91 when the surface effect exists, we chose GGA+PW91, not GGA+PBE, in present calculations due to only bulk properties being considered.
In fact, we also had verified the Li_2SiO_3 lattice parameters and bulk modulus difference resulted from GGA+PBE and GGA+PW91 scheme and found it was so much small that it

Table 2: Experimental and optimized theoretical atomic fractional coordinates for Li_2SiO_3 and charge Mulliken populations

Atom	Wyckoff site	Expt.	Calc.	Total	Net
Li	8b	(0.1740,0.3441,0.0045)	(0.1739,0.3443,0.0047)	2.07	0.93
Si	4a	(0,0.1731,0.5008)	(0,0.1705,0.5009)	2.09	1.91
O1	8b	(0.1457,0.3108,0.4176)	(0.1436,0.3078,0.4209)	7.30	-1.30
O2	4a	(0,0.1179,0.8598)	(0,0.1122,0.8526)	7.17	-1.17

could be canceled. However, the crystal binding energy from PW91 is about 2.2 eV lower than that from PBE. That is to say lower total energy calculated from PW91 comparing with that from PBE.

Fig. 3 just illustrated the above dependence relationship of Li_2SiO_3 for simplifying description because the variations of binding energy with energy cut off values are similar for both lithium silicates within LDA + LZ-CP, GGA + PBE and GGA + PW91 scheme. As shown in Fig. 3, the calculated binding energy values slightly increased as energy cut off increased from 340 to 600 eV under LDA + LZ-CP, GGA within both PBE and PW91 schemes. At every energy cut off, the binding energy from LDA + LZ-CP is the lowest and from PW91 is about 2.2 eV lower than that from PBE. On the other hand, in Fig.4 we also plotted the relationships between cell parameters and energy cut off values for Li_2SiO_3, a very tiny variation of calculated values are obtained within different scheme. It is found that, although the variation is tiny, the longest (a,b,c) and largest cell volume are obtained for energy cut off 340 eV within LDA, GGA+PBE and GGA+PW91 schemes. The calculated lattice parameters oscillated slightly as energy cut off increased from 400 to 600 eV. Therefore, our conclusions are reasonable when we used the value of 400 eV for the stability structural and electronic investigations calculations in this paper.
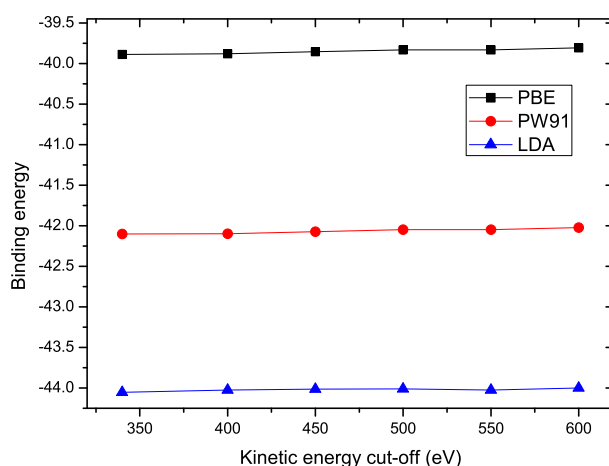
Figure 3: The calculated binding energy of Li_2SiO_3 as a function of energy cutoff values. The LDA + LZ-CP, GGA + PBE and GGA + PW91 scheme were used and compared.

First we illustrated the calculated equilibrium lattice parameters in Table 1. It should be noted that here the energy cut off was valued as 400 eV and the GGA + PW91 scheme was adopted. When compared with experimental values in Table 1, theoretical parameters all elongate parallel to x-, y-, and z-axis for Li_2SiO_3 and Li_4SiO_4 structure, the β is slightly reduced for Li_4SiO_4. When using GGA + PW91 scheme, the deviation between experimental and evaluated values of cell parameters is varied as 0.97%, 1.0% and 1.1% along x, y and z directions for Li_2SiO_3. Similarly, it is varied as 1.6%, 0.03% and 0.93% along x, y and z directions for Li_4SiO_4, respectively. Within LDA + LC-PZ scheme, theo-
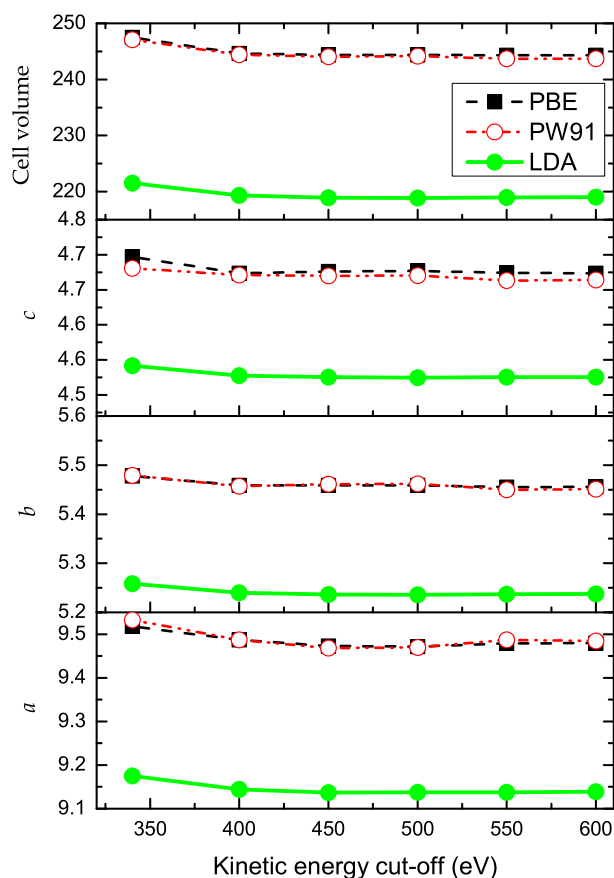
Figure 4: The variations of cell parameters of Li_2SiO_3 as a function of energy cut-off values. The unit of a, b, and c is Å, the unit of cell volume is $Å^3$.

retical parameters all contract, the deviation is changed as -2.7%, -2.9% and -1.8% along x, y and z directions for Li_2SiO_3. As for GGA, lattice expansions are the common results [42, 43]. The effects of energy cut off on calculated equilibrium lattice parameters are complicate as illustrated in Fig. 4. In Li_2SiO_3, the $Si-O_1$ bond length is 1.599 Å, and $Si-O_2$ is 1.688 Å and 1.692 Å, slight shorter than the experimental values, respectively. The $Li-O_1$ bond length is 1.925 Å, 1.931 Å, and 1.954 Å, respectively. The closest $Li-O_2$ bond length is 2.194 Å. The calculated atomic parameters of Li_2SiO_3 are also shown in Table 2. The results indicate that the calculated coordinates of Li, Si and O atoms were consistent with the experimental values.

While in Li_4SiO_4, the comparison of calculated atomic coordinates and experimental measurements were given in Table 3. It can be seen that the optimized coordinates of Li, Si and O atoms have not change significantly, especially in y axis. Our calculation results are consistent with the coordinates given by Munakata *et al.* [32]. The Si-O bond length and O-Si-O bond angle for every SiO_4 tetrahedra are listed in Table 4.

Table 3: Experimental and optimized theoretical atomic fractional coordinates for Li_4SiO_4 and charge Mulliken populations

Atom	Site	Expt.	Calc.	Total	Net
Si 1	2 e	(0.3416,0.25,0.0056)	(0.3403,0.25,0.0073)	12.38	1.62
Si 2	2 e	(0.7540,0.25,0.1386)	(0.7546,0.25,0.1373)	12.39	1.61
Si 3	2 e	(0.4772,0.25,0.7152)	(0.4754,0.25,0.7150)	12.38	1.62
Si 4	2 e	(0.2003,0.25,0.2924)	(0.2045,0.25,0.2941)	12.39	1.61
Si 5	2 e	(0.0406,0.25,0.5773)	(0.0396,0.25,0.5792)	12.39	1.61
Si 6	2 e	(0.8941,0.25,0.8567)	(0.8938,0.25,0.8557)	12.33	1.67
Si 7	2 e	(0.6145,0.25,0.4280)	(0.6152,0.25,0.4281)	12.42	1.58
O 1	4 f	(0.3560,0.0265,0.0579)	(0.3575,0.0295,0.0611)	7.00	-1.00
O 2	4 f	(0.7860,0.0342,0.1956)	(0.7881,0.0348,0.1953)	7.00	-1.00
O 3	4 f	(0.4994,0.0305,0.7715)	(0.4953,0.0314,0.7704)	6.98	-0.98
O 4	4 f	(0.2185,0.0283,0.3484)	(0.2199,0.0283,0.3472)	6.98	-0.98
O 5	4 f	(0.0668,0.0316,0.6344)	(0.0665,0.0350,0.6382)	6.98	-0.98
O 6	4 f	(0.9269,0.0330,0.9175)	(0.9261,0.0354,0.9147)	6.98	-0.98
O 7	4 f	(0.6530,0.0283,0.4811)	(0.6539,0.0311,0.4805)	6.99	-0.99
O 8	2 e	(0.1998,0.25,0.9638)	(0.2013,0.25,0.9622)	6.99	-0.99
O 9	2 e	(0.6186,0.25,0.0977)	(0.6207,0.25,0.0978)	6.97	-0.97
O10	2 e	(0.3352,0.25,0.6744)	(0.3344,0.25,0.6750)	7.00	-1.00
O11	2 e	(0.0626,0.25,0.2447)	(0.0658,0.25,0.2483)	7.00	-1.00
O12	2 e	(0.9082,0.25,0.5278)	(0.9099,0.25,0.5295)	7.00	-1.00
O13	2 e	(0.7611,0.25,0.8143)	(0.7618,0.25,0.8120)	6.99	-0.99
O14	2 e	(0.4745,0.25,0.3985)	(0.4775,0.25,0.3949)	6.99	-0.99
O15	2 e	(0.4194,0.25,0.9341)	(0.4189,0.25,0.9359)	6.98	-0.98
O16	2 e	(0.8436,0.25,0.0682)	(0.8454,0.25,0.0716)	7.00	-1.00
O17	2 e	(0.5526,0.25,0.6386)	(0.5536,0.25,0.6433)	6.98	-0.98
O18	2 e	(0.2842,0.25,0.2228)	(0.2831,0.25,0.2232)	7.00	-1.00
O19	2 e	(0.1308,0.25,0.5114)	(0.1322,0.25,0.5165)	6.98	-0.98
O20	2 e	(0.9918,0.25,0.7957)	(0.9879,0.25,0.7923)	6.98	-0.98
O21	2 e	(0.6967,0.25,0.3561)	(0.6932,0.25,0.3533)	7.00	-1.00
Li 1	4 f	(0.3823,0.0072,0.4068)	(0.3833,0.0043,0.4091)	2.41	0.59
Li 2	4 f	(0.8123,0.0006,0.5448)	(0.8119,0.0035,0.5448)	2.43	0.57
Li 3	4 f	(0.6605,0.0112,0.8270)	(0.6621,0.0073,0.8262)	2.42	0.58
Li 4	4 f	(0.5255,0.9981,0.1173)	(0.5247,0.9921,0.1161)	2.42	0.58
Li 5	2 e	(0.2722,0.25,0.8558)	(0.2720,0.25,0.8612)	2.50	0.50
Li 6	2 e	(0.4176,0.25,0.5491)	(0.4138,0.25,0.5523)	2.41	0.59
Li 7	2 e	(0.1321,0.25,0.1464)	(0.1314,0.25,0.1480)	2.38	0.62
Li 8	2 e	(0.9695,0.25,0.4271)	(0.9730,0.25,0.4301)	2.43	0.57
Li 9	2 e	(0.4490,0.25,0.278)	(0.4549,0.25,0.2783)	2.43	0.57
Li10	2 e	(0.7272,0.25,0.6977)	(0.7254,0.25,0.6944)	2.50	0.50
Li11	2 e	(0.5940,0.25,0.9794)	(0.5898,0.25,0.9817)	2.41	0.59
Li12	4 f	(0.1962,0.9631,0.0192)	(0.1923,0.9706,0.0148)	2.34	0.66
Li13	4 f	(0.3309,0.9681,0.7279)	(0.3316,0.9648,0.7324)	2.42	0.58
Li14	4 f	(0.9515,0.0298,0.7108)	(0.9446,0.0307,0.7049)	2.39	0.61
Li15	4 f	(0.0790,0.0278,0.8663)	(0.0736,0.4908,0.8632)	2.40	0.60
Li16	4 f	(0.2373,0.0379,0.5977)	(0.2397,0.0394,0.5979)	2.39	0.61
Li17	2 e	(0.1407,0.25,0.7360)	(0.1341,0.25,0.7321)	2.38	0.62
Li18	2 e	(0.0082,0.25,0.0076)	(0.0058,0.25,0.0096)	2.43	0.57
Li19	2 e	(0.8701,0.25,0.2956)	(0.8840,0.25,0.2843)	2.43	0.57

It reveals that Si-O bond length ranges from 1.576 Å to 1.656 Å, which are slightly shorter than the experimental values, and O-Si-O bond angle varies from 105.3° to 114.3°. In one SiO_4 tetrahedra, the bond length of Si-O1 equals to Si-O2, and the bond angle of O1-Si-O3 and O1-Si-O4 equals to that of O2-Si-O3 and O2-Si-O4, respectively.

3.2 Electronic structures

In this part, the calculated electronic structure will be discussed. The calculated electronic band structures of Li_2SiO_3 and Li_4SiO_4 are shown in Fig. 5 (a) and (b), respectively. The separated conduction band (CB) and valence band (VB) are obtained with indirect band gap of 5.36 eV Li_2SiO_3 and direct band gap of 5.53 eV for Li_4SiO_4, respectively, in this work. It is very easy to understand that the non-conductive nature for these two lithium silicates. However, the band gap of Li_2SiO_3 and Li_4SiO_4 is lower than the reference value obtained by Ching *et al*. [31] and Munakata *et al*. [32], respectively. In CASTEP, the plane wave basis sets and ultrasoft-pseusopotential are used to represent the wave functions of electrons and only the electrons of $Li(1s^22s^1)$, $Si(3s^23p^2)$ and $O(2s^22p^4)$ are considered in calculation. While in CRYSTAL98, the all-electron Gaussian-type basis sets are adopted to describe the wave functions of electrons, it can produce more fine structure and detailed information of electronic distributions. As discussed in Duan's work [42], the DFT underestimates the excited-state energies and the calculated band gaps are usually smaller than the experimental measurements.
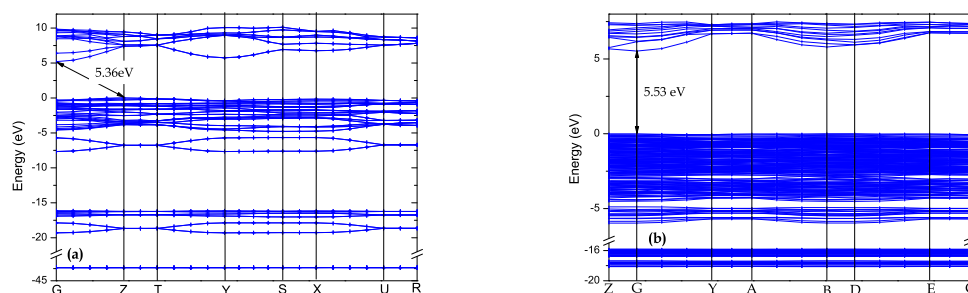
Figure 5: The calculated electronic band structures of (a) Li_2SiO_3 and (b) Li_4SiO_4.

Here we mainly focus our concerning on the valence band density of states and electron density distribution maps for studied structures. The total density of states (TDOS) of Li_2SiO_3 and Li_4SiO_4 and partial density of states (PDOS) of Li, Si, and O atoms are shown in Fig. 6. The Fermi energy was assumed to be the zero energy level. These data are broaden with a 0.15 eV full width at half height (FWHH) Gaussian. In Fig. 6 (a), it is evident that Li_2SiO_3 bulk ground properties are mainly determined by $2p$ orbital electrons of oxygen atoms. $3s$ and $3p$ bands of silicon atoms are low in energy and overlaped

Table 4: Optimized theoretical Si-O bond length and O-Si-O bond angle for every SiO$_4$ tetrahedra within Li$_4$SiO$_4$

Atom	Site	Calculated position	Si-O bond length (Å)	O-Si-O bond angle (°)
Si 1	2 e	(0.3403,0.25,0.0073)	Si-O1=1.608 Si-O2=1.608 Si-O3=1.610 Si-O4=1.656	∠O1-Si-O2=113.23 ∠O1-Si-O3=112.23 ∠O1-Si-O4=105.88 ∠O2-Si-O3=112.23 ∠O2-Si-O4=105.88 ∠O3-Si-O4=106.72
Si 2	2 e	(0.7546,0.25,0.1373)	Si-O1=1.636 Si-O2=1.636 Si-O3=1.635 Si-O4=1.578	∠O1-Si-O2=106.51 ∠O1-Si-O3=106.25 ∠O1-Si-O4=111.46 ∠O2-Si-O3=106.25 ∠O2-Si-O4=111.46 ∠O3-Si-O4=114.39
Si 3	2 e	(0.4754,0.25,0.7150)	Si-O1=1.615 Si-O2=1.615 Si-O3=1.610 Si-O4=1.654	∠O1-Si-O2=111.07 ∠O1-Si-O3=112.27 ∠O1-Si-O4=105.51 ∠O2-Si-O3=112.27 ∠O2-Si-O4=105.51 ∠O3-Si-O4=109.74
Si 4	2 e	(0.2045,0.25,0.2941)	Si-O1=1.607 Si-O2=1.607 Si-O3=1.604 Si-O4=1.656	∠O1-Si-O2=114.28 ∠O1-Si-O3=112.33 ∠O1-Si-O4=105.32 ∠O2-Si-O3=112.33 ∠O2-Si-O4=105.32 ∠O3-Si-O4=106.39
Si 5	2 e	(0.0396,0.25,0.5792)	Si-O1=1.636 Si-O2=1.636 Si-O3=1.612 Si-O4=1.586	∠O1-Si-O2=106.32 ∠O1-Si-O3=107.99 ∠O1-Si-O4=112.46 ∠O2-Si-O3=107.99 ∠O2-Si-O4=112.46 ∠O3-Si-O4=109.41
Si 6	2 e	(0.8938,0.25,0.8557)	Si-O1=1.641 Si-O2=1.641 Si-O3=1.634 Si-O4=1.576	∠O1-Si-O2=105.59 ∠O1-Si-O3=106.09 ∠O1-Si-O4=112.52 ∠O2-Si-O3=106.09 ∠O2-Si-O4=112.52 ∠O3-Si-O4=113.42
Si 7	2 e	(0.6152,0.25,0.4281)	Si-O1=1.615 Si-O2=1.615 Si-O3=1.652 Si-O4=1.595	∠O1-Si-O2=111.26 ∠O1-Si-O3=105.66 ∠O1-Si-O4=110.98 ∠O2-Si-O3=105.66 ∠O1-Si-O3=110.98 ∠O1-Si-O3=112.06
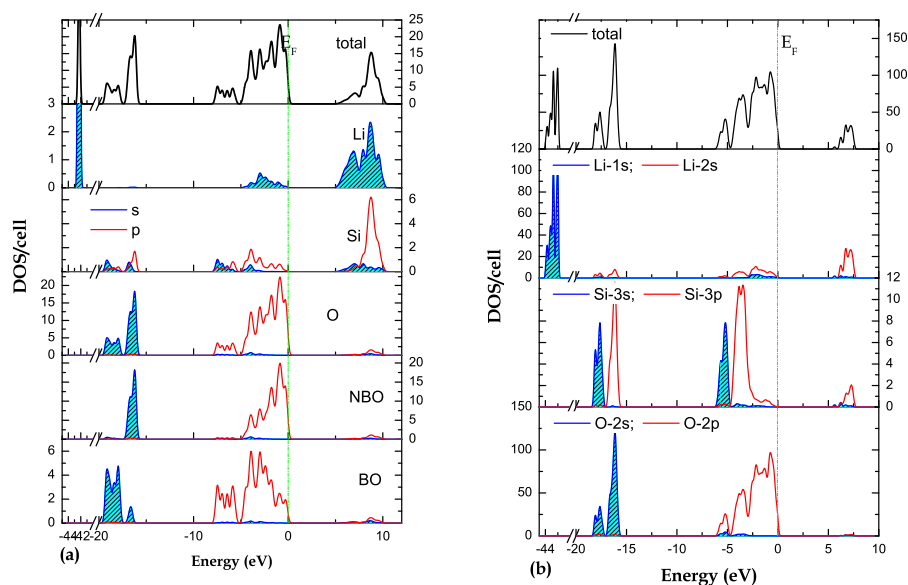
Figure 6: The calculated total densities of states and PDOS of Li, Si, and O atoms in the crystal of (a) Li_2SiO_3 and (b) Li_4SiO_4.

each other in some degrees. Strong peaks occur at -0.93, -1.89, -3.14 and -4.06 eV in the valence band and the oxygen 2s peak occurs at -15.87 and -19.10 eV. Ching *et al*. [23] reported similar results except for small difference in energy value. They gave the strong peaks occur at -0.82, -3.02 and -5.35 eV in the valence band and the oxygen 2s peak occurs at -16.26 with a shoulder at -17.58 eV [23]. From the PDOS of Li, Si and O atoms in Li_2SiO_3, we can observe that the upper valence band is mainly composed of O 2*p* and Si 3*p* orbital, and the lower VB is mainly contributed from O 2*s*, Si 3*s*3*p* and Li 2s orbital. The Li 1*s* orbital electrons shows very localization and distribute at the lowest energy level of -43 eV. We can see that there is no other orbital electrons from oxygen and silicon atoms overlap here. From the lower two parts of Fig. 6 (a), the bridging oxygen (BO) and non-bridging oxygen (NBO) atoms showed different electronic density of state. The electrons of BO tend to distribute at upper valence band closing to the Fermi level, while those of NBO distributes at lower energy and split into double peaks. As we known, the NBO atoms not only covalent with silicon atom, but also bond to the lithium atoms around them in ionized bonding and partial covalence bonding. Their electronic density of sates exhibit more complicate. The covalency in these two crystals is mainly caused by O 2*s* and Si 3*p* hybridizations.

The TDOS of Li_4SiO_4, from Fig. 6(b), strong peaks occur at -0.74, -2.15, -3.45 and -5.20 eV in the valence band and the oxygen 2s peak occurs at -16.15 and -17.62 eV. The -0.74 and -2.15 eV peaks mainly result from the contributions of O 2*p* and Li 2s orbital, -3.45 eV

peak comes from the O $2p$, Si $3p$ and Li $2s$ orbital, while -5.20 eV is composed of O $2p$, Si $3s$ and Li $2s$ orbital. For strong peak at -16.15 eV, it results from the contribution of O $2s$, Si $3p$ and Li $2s$, while at -17.62 eV it comes from O $2s$, Si $3s$ and Li $2s$ orbitals. We observe that partial Li $1s$ orbital electrons also participate in bonding with O $2p$ electrons. So the Li $1s$ orbital electrons locating at the lowest energy level split into multi-peaks. This is not observed in calculated DOS of Li_2SiO_3 crystal.

3.3   Electron populations analysis

It should be noted that, in the Mulliken population analysis, the net charges were computed by subtracting the atomic number from the total charge.
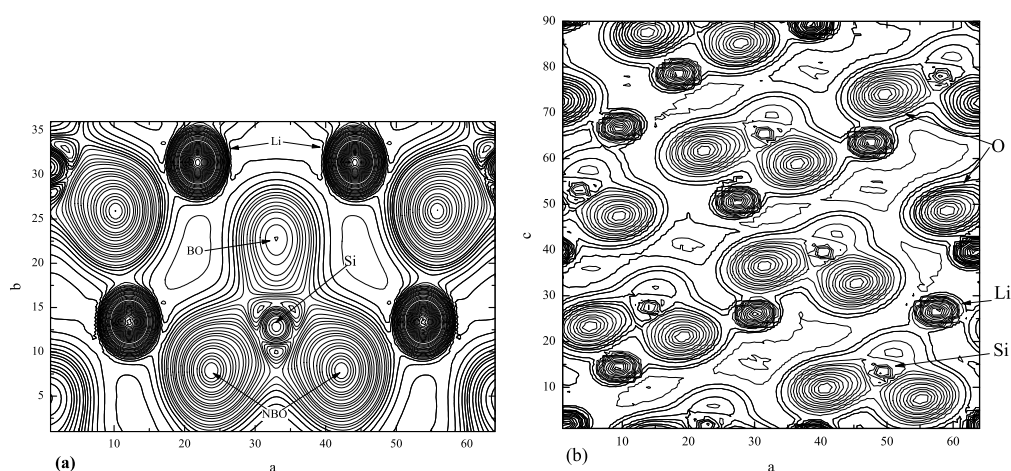
Figure 7: Total electron density distribution contour of (a) Li_2SiO_3 (0 0 1) plane and (b) Li_4SiO_4 (0 1 0) plane. The density value is from 0 to 2600 and 0 to 1.3×10^4 electrons/$\mathring{A}^3$ for Li_2SiO_3 and Li_4SiO_4, respectively.

The Mulliken charges of Li ,Si and O atoms in Li_2SiO_3 are listed in Table 2. The net charge of Li is +0.93 (in the total charge of 2.07), and thus Li atoms appear to be present as almost ionic states. However, it losses slight fewer electron than that of a real Li^{+1} ion. Other than Li, the net charge of Si is +1.91 (in the total charge, 12.09), while the net charge of O is -1.17 and -1.30 (in the total charge, 9.17 to 9.30) for the BO O1 and NBO O2, respectively. It can be seen that the non-bridging O atoms exhibits more electronegative than the bridging O atoms. In Section 2, it has been described that there are three closest Li atoms around every NBO, but only one Li atom around every BO. The calculated electron population of Li atoms reveals that all the Li atoms have the same net charge of +0.6893. So, the electrons transferred from Li atom to the NBOs should be more than those to the BOs. Clearly, the Si-O bond shows covalent characteristic. However, the strength of Si-O_1 and Si-O_2 is different due to their different bonding environment. From Fig. 6(a), the DOS of NBO and BO shows appreciative difference that the electrons of BO populate at higher energy level and closer to Fermi level than those of NBO. The total

electron density map of (0 0 1) plane is shown in Fig. 7. The representative locations of Li, Si and O atoms are pointed with the arrows in the figure, and other locations can be deduced from the similarity in the arrangements of Si and O atoms. Electron densities increase more steeply around Si and Li atom sites compared with that around O atoms. The electronic density difference map of (0 0 1) plane is shown in Fig. 8 (a). It reveals that electrons of Si transfers to O atoms.
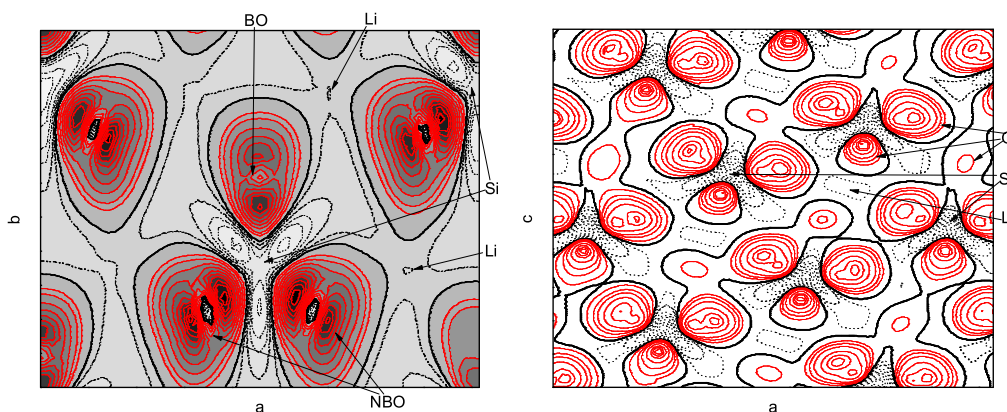
Figure 8: Electron density difference of Li_3SiO_3 (0 0 1)[left] Li_4SiO_4 (0, 1/4, 0) plane [right]. The unit of density value is electrons/Å^3.

The Mulliken charges of Li ,Si and O atoms in Li_4SiO_4 are listed in Table 3. The net charge of Li ranges from 0.50 to 0.66 (in the total charge, 2.50 to 2.34) with a mean value of +0.59, which is lower than that of Li_3SiO_3. Other than Li, the net charge of Si ranges from +1.58 to +1.67 (in the total charge, 12.34 to 12.42) with a mean value of +1.62, while the net charge of O ranges from -1.00 to -0.97 (in the total charge, 6.97 to 7.00) with a mean value of -0.99. These net charges are well consistent with the results for $Li_1H_3SiO_4$ cluster given by Nakazawa *et al*. [31]. In their study, Gaussian 94 with the 6-311G basis set was used and suggests that the net charges of Li, Si, and O are +0.691, +1.596 and -0.99, respectively. However, Munakata *et al*. [25] reported that the net charges of Li, Si and O range from +0.881 to +0.913, +1.343 to +2.119, and -1.307 to -1.151, respectively. In their calculations, CRYSTAL98 program with Gaussian basis set 6-1G for Li, 6-21G for Si and 6-21G* for O are used. In comparison with their result, less charge transfer for Li, Si and O is observed in the result of present study. According to the structure of Li_4SiO_4, as shown in Table 4, all Si atoms in the crystal structure have four neighboring O atoms within the distance of 1.656 Å. The majority of neighboring atoms of Li atoms within the distance of 2.384 Åare O atoms but Si atoms are not included. The results of the Mulliken analysis for neighboring atoms suggest that the overlap populations of Si-O (within 1.656 Å) and Li-O (within 2.384 Å) range 0.58 to 0.74 and -0.03 to 0.24, respectively. The overlap populations of the most neighboring Li-Li is less than -0.82. The lower overlap population density for Li-O and Li-Li coincides with the results obtained in the SCF calculation for the Li_2O crystal [20].

3.4 Mechanical properties

Finally, the mechanical properties of these compounds will be briefly discussed in this part. In order to simplify the calculation, the same k point and GGA-PW91 exchange correlation scheme as electronic structure calculation was used. All of elastic constants are summarized in Tables 5 and 6.

$$\sigma_{ij} = C_{ijkl}\varepsilon_{kl} \tag{2}$$

Table 5: Calculated elastic constants

Species	C_{ij}												
	C_{11}	C_{12}	C_{13}	C_{15}	C_{22}	C_{23}	C_{25}	C_{33}	C_{35}	C_{44}	C_{46}	C_{55}	C_{66}
Li_2SiO_3	146.5	48.8	52.4		134.5	49.3		154.0		71.6		55.7	36.9
Li_4SiO_4	119.5	28.7	34.5	2.5	141.7	43.2	-12.0	144.8	-1.2	67.7	-48.3	48.2	33.0

Table 6: Calculated bulk modulus B, Young modulus E, and shear modulus G.

Species	B(GPa)	E(GPa)			G(GPa)
		E_x	E_y	E_z	
Li_2SiO_3	81.5	120.1	110.8	126.7	51.8
Li_4SiO_4	67.6	108.2	122.7	125.8	49.8

The independent elastic constants number usually depends on the symmetry properties of crystal class according to Neumann's rule. Concretely speaking, it is closely related to 32 point groups and transformation matrix elements for a tensor with a rank of 4. The fundamental theory behind elastic constant evaluations is Hook's law: a linear relationship between two tensors, stress and strain, and a proportional coefficient C_{ijkl}. In CASTEP code, in order get each independent elastic constant value, appropriate number of strain patterns will be imposed on crystal cell. The total energy associated with each strain pattern is optimized and then fitted with [43–46]

For orthorhombic and monoclinic crystal structures of Li_2SiO_3 and Li_4SiO_4, there are nine (i.e. C_{11}, C_{12}, C_{13}, C_{22}, C_{23}, C_{33}, C_{44}, C_{55} and C_{66}) and thirteen (i.e. C_{11}, C_{12}, C_{13}, C_{15}, C_{22}, C_{23}, C_{25}, C_{33}, C_{35}, C_{44}, C_{46}, C_{55} and C_{66}) independent C_{ijkl} values, respectively. Bulk modulus, Young modulus and shearing modulus values are directly calculated within these constants. The calculated isothermal bulk modulus of Li_2SiO_3 and Li_4SiO_4 is 81.5 GPa and 67.6 GPa, respectively. Since orthorhombic and monoclinic structure have lower symmetry than cubic class. Consequently, Young modulus is anisotropy at x-y, y-z and x-z plane. The calculated Young modulus values along x,y,z axis are different for both lithium silicates. For Li_2SiO_3 it is 120.1, 110.7 and 126.7 GPa along x-, y- and z-axis, while for Li_4SiO_4 it is 108.2, 122.7 and 125.8 GPa, respectively. The evaluated elastic constants matrix of Li_2SiO_3 has positive values which indicate that it is mechanically stable structures. However, among the calculated elastic constants matrix of Li_4SiO_4 three elastic constants, C_{25}, C_{35} and C_{46}, are negative. It revealed that Li_4SiO_4 might be mechanically unstable in some degrees. The real reasons for this mechanically unstable should be verified by the further investigations using the different functinals and pseudopotentials.

4 Conclusions

We demonstrate that the first principle calculation within GGA-PW91 functional as implemented in CASTEP code is applicable to study the crystalline and electronic properties of lithium silicates. We carried out the calculations of the crystalline and electronic properties of lithium silicate bulks using the first principle calculation within GGA as implemented in CASTEP code. The results of electron density of state (DOS) and project DOS (PDOS) reveal the insulating nature of lithium silicates with band gap of 5.36 and 5.53 eV for Li_2SiO_3 and Li_4SiO_4, respectively. Simultaneously, the covalency properties mainly resulted from the overlapping of O $2p$ and Si $3p$ band. Two types of oxygen, non-bridging O (NBO) atoms and bridging O (BO) atoms, in Li_2SiO_3 show significantly different $2p$ orbital electron distributions. It is found that the Si $3s$ and $3p$ hybrids in Li_2SiO_3, but not in Li_4SiO_4. In both lithium silicates, the electronic density increased more steeply around Li and Si atom sites compared with that around O atoms.

References

 [1] C. E. Johnson, J. Nucl. Mater. 179-181 (1991) 42.
 [2] C. E. Johnson, Ceramics Int. 17 (1991) 253.
 [3] C. E. Johnson, J. Nucl. Mater. 270 (1999) 212.
 [4] N. Roux, G. Hollenberg, C. Johnson, *et al.*, Fusion Eng. Des. 27 (1995) 154.
 [5] Y. Ishii, Y. Morii, R. M. Nicklow, *et al.*, Physica B 213-214 (1995) 436.
 [6] T. Terai, H. Mohri, and Y. Takahashi, J. Nucl. Mater. 178-181 (1991) 808.
 [7] C. Alvani, P. L. Carconi, S. Casadio, *et al.*, J. Nucl. Mater. 289 (2001) 303.
 [8] T. Kinjyo, M. Nishikawa, M. Enoeda, and S. Fukad, Fusion Eng. Des. 83(4) (2008) 580.
 [9] A. La Barbera, B. Riccardi, A. Donato, *et al.*, Fusion Eng. Des. 294 (2001) 223.
[10] S. Beloglazov, M. Nishikawa, M. Glugla, *et al.*, J. Nucl. Mater. 329-333 (2004) 1274.
[11] S. Akahori, E. Tega, Y. Morimoto, *et al.*, J. Radioanaly. Nucl. Chem. 255 (2003) 257.
[12] T. Kinjyo, M. Nishikawa, and M. Enoeda, J. Nucl. Mater. 367-370 (2007) 1361.
[13] Y. W. Rhee, J. H. Yang, and K. S. Kim, Thermochimica Acta 455 (2007) 86.
[14] Y. Nishikawa, M. Oyaidzu, and A. Yoshikawa, J. Nucl. Mater. 367-370 (2007) 1371.
[15] M. Nishikawa, T. Kinjyo, and Y. Nishida, J. Nucl. Mater. 325 (2004) 87.
[16] T. Kinjyo, M. Nishikawa, N. Yamashita, *et al.*, Fusion Eng. Des. 82 (2007) 2147.
[17] K. Hashimoto, M. Nishikawa, N. Nakashima, *et al.*, Fusion Eng. Des. 61-62 (2002) 375.
[18] A. Shluger and N. Itoh, J. Phys.: Condens. Matter 2 (1990) 4119 .
[19] H. Tanigawa and S. Tanaka, J. Nucl. Mater. 307-311 (2002) 1446 .
[20] R. Dovesi, C. Roetti, M. Freyria-Fava, *et al.*, Chem. Phys. 156 (1991) 11.
[21] A. Lichanot, M. Gelize, C. Larrieu, and C. Pisani, J. Phys. Chem. Solids 52 (1991) 1155.
[22] A. De Vita, M. J. Gillan, J. S. Lin, *et al.*, Phys. Rev. Lett. 68 (1992) 3319.
[23] A. Sutjianto, S. W. Tam, R. Pandey, *et al.*, J. Nucl. Mater. 219 (1995) 250.
[24] R. Shah, A. De Vita, and M. C. Payne. J. Phys.: Condens. Matter 7 (1995) 6981.
[25] P. Sony and A. Shukla, Phys. Rev. B 77 (2008) 075130.

[26] L. Padilla-Campos, J. Mol. Struct. (Theochem.) 580 (2002) 101.
[27] L. Padilla-Campos, J. Mol. Struct. (Theochem.) 621 (2003) 107.
[28] T. Nakazawa, K. Yokoyama, and K. Noda, J. Nucl. Mater. 258 (1998) 571.
[29] T. Nakazawa, K. Yokoyama, V. Grismanovs, and Y. Katano, J. Nucl. Mater. 279 (2000) 201.
[30] T. Nakazawa, K. Yokoyama, V. Grismanovs, and Y. Katano, J. Nucl. Mater. 297 (2001) 69.
[31] W. Y. Ching, Y. P. Li, B. W. Veal, *et al.*, Phys. Rev. B 32 (1995) 1203.
[32] K. Munakata and Y. Yokoyama, J. Nucl. Sci. & Technol. 38 (2001) 915.
[33] H. Völlenkle, Z. Kristallogr. 154 (1981) 77.
[34] H. Völlenkle, A. Wittmann, and H. Nowtony, Monatsh. Chem. 99 (1968) 1360.
[35] D. Tranqui, R. D. Shannon, H. -Y. Chen, *et al.*, Acta. Cryst. B 35 (1979) 2479.
[36] M. D. Segall, P. J. D. Lindan, M. J. Probert, *et al.*, J. Phys.: Condens. Matter 14 (2002) 2717.
[37] A. E. Mattsson, P. A. Schultz, M. P. Desjarlais, *et al.*, Model. Simul. Mater. Sci. Eng. 13 (2005) R1.
[38] V. Milman, B. Winkler, J. A. White, *et al.*, Int. J. Quant. Chem. 77 (2000) 895.
[39] W. Kohn, Rev. Mod. Phys. 71 (1999) 1253 .
[40] J. P. Perdew, K. Burke, and W. Ernzerhof, Phys. Rev. Lett. 77 (1996) 3865.
[41] B. Pfrommer, G. M. Cote, S. G. Louie, *et al.*, J. Comput. Phys. 131 (1997) 133.
[42] Y. Duan and D. C. Sorescu, Phys. Rev. B 79 (2009) 014301.
[43] L. Fast, J. M. Wills, B. Johansson, and O. Eriksson, Phys. Rev. B 51 (1995) 17431.
[44] P. SÖderlind, O. Eriksson, J. M. Wills, and A. M. Boring, Phys. Rev. B 48 (1993) 5844.
[45] N. W. Ashcroft and N. D. Mermin, Solid State Physics(Saunders College, Philadelphia, 1976).
[46] J. E. Lowther, Physica B 322 (2002) 173.